Computers and Concrete, *Vol. 13, No. 4 (2014) 547-567*
DOI: http://dx.doi.org/10.12989/cac.2014.13.4.547

Optimum seismic design of unbonded post-tensioned precast concrete walls using ANN

Jamal A. Abdalla*[1], Elias I. Saqan[2] and Rami A. Hawileh[1]

[1]*Department of Civil Engineering, American University of Sharjah, UAE*
[2]*Department of Civil Engineering, American University in Dubai, UAE*

(*Received August 5, 2013, Revised January 1, 2014, Accepted January 14, 2014*)

Abstract. Precast Seismic Structural Systems (PRESSS) provided an iterative procedure for obtaining optimum design of unbonded post-tensioned coupled precast concrete wall systems. Although PRESSS procedure is effective, however, it is lengthy and laborious. The purpose of this research is to employ Artificial Neural Network (ANN) to predict the optimum design parameters for such wall systems while avoiding the demanding iterative process. The developed ANN model is very accurate in predicting the non-dimensional optimum design parameters related to post-tensioning reinforcement area, yield force of shear connectors and ratio of moment resisted by shear connectors to the design moment. The Mean Absolute Percent Error (MAPE) for the test data for these design parameters is around %1 and the correlation coefficient is almost equal to 1.0. The developed ANN model is then used to study the effect of different design parameters on wall behavior. It is observed that the design moment and the concrete strength have the most influence on the wall behavior as compared to other parameters. Several design examples were presented to demonstrate the accuracy and effectiveness of the ANN model.

Keywords: seismic design; precast concrete wall; unbonded post-tensioned; neural network; PRESSS

1. Introduction

The dominant type of concrete buildings in moderate and high seismic zones is the conventional reinforced concrete (RC) structural system with monolithic Cast-in-Place (CIP) shear walls and moment resisting frames. Until recently precast/prestressed (pre-tensioned or post-tensioned) concrete buildings with jointed connections were seldom used in moderate and high seismic zones. The reason is that the prevailing view is that they are not suitable structural systems for buildings in moderate and high seismic zones. In the last two decades (Priestley 1991), an ambitious research program, termed Precast Seismic Structural Systems (PRESSS), was launched to explore the viability of using precast/prestressed concrete buildings in zones of high seismic activities, to study and predict the performance of properly designed precast concrete buildings under seismic response, and to highlight the major advantages of seismic performance of precast concrete buildings in incurring less damage as compared to conventional reinforced concrete buildings (Priestley 1996, Priestley *et al*. 1999). In addition, the objective of the PRESSS program

*Corresponding author, Ph.D., E-mail: jabdalla@aus.edu

http://www.techno-press.org/?journal=cac&subpage=8 ISSN: 1598-8198 (Print), 1598-818X (Online)

was to develop design guidelines that are appropriate to use in various seismic zones and to be incorporated into design codes (Nakaki *et al*. 1999; Stanton and Nakaki 2002; Ghosh and Hawkins 2003). As a result, the design of special precast concrete shear walls was included in the 2003 edition of NEHRP Recommended Provisions for Seismic Regulations of New Buildings and other Structures (Hawkins and Ghosh 2004) and the ACI Innovation Task Group (ACI ITG-5.2-09).

In phase III of the PRESSS research program five different structural seismic systems made from precast concrete members were tested and the structural wall system with post-tensioned reinforcement and special damping shear connectors between wall panels was the most promising. This system was designed using the Direct Displacement-Based Design (DDBD) procedure. The DDBD procedure allows structures to be designed to respond in the design-level earthquake to specified displacement limits to control damage while taking into consideration the inherit ductility and damping characteristics of the structural system (Priestley 2002). For precast buildings the procedure was able to take advantage of the unique properties of precast/prestressed concrete using dry jointed construction (Nakaki *et al*. 1999). The DDBD procedure has many advantages compared to the conventional and widely used Force-Based Design (FBD) procedure, especially when designing precast post-tensioned jointed structural systems. Both procedures, the DDBD and the FBD, are iterative. The DDBD procedure requires iteration by revising the damping to determine the effective period from the design displacement response spectra while the FBD procedure requires iteration by revising the stiffness to estimate the elastic period (Priestley 2002). In addition, the FBD procedure is not suitable for precast post-tensioned wall systems because they represent the behavior of jointed precast systems poorly and because they do not emulate monolithic concrete structures (Nakaki *et al*. 1999). Both DDBD and FBD are iterative processes that require tedious and lengthy calculations to achieve optimum design values of post-tensioning reinforcement area and total shear force in connectors. As a result, a simplified non-iterative design procedure was proposed by Sritharan and Aaleti (2006) and Aaleti and Sritharan (2009) for design of such wall systems. The proposed procedure was adopted by ACI ITG-5.2-09 (2009) guidelines with minor modifications. The ACI ITG-5.2-09 design procedure does not ensure an optimum combination of the shear connectors force and post-tensioning reinforcement area (post-tensioning force). In addition, the ACI ITG-5.2-09 design procedure calculates the required area of post-tensioning reinforcement based on the design moment for the wall panel resisting the larger or largest moment (the leading wall in a two-wall panels system and an intermediate wall in a three- or more wall panels system) which results in conservative amounts of post-tensioning reinforcement area.

Saqan and Hawileh (2010) developed a non-dimensional design procedure and a set of non-dimensional design charts that require no iterations for the design of such a wall system. The developed charts yield an optimum design in which the moment capacity of the wall is equal to the applied design moment while a zero residual drift is maintained in the system. Bhunia *et al*. (2012) developed a design technique for symmetrical coupled shear walls under seismic motion. They validated the developed design technique with nonlinear analysis programs and carried out parametric study to find out the limitations along with remedial action of their design technique. Hawileh *et al*. (2013) developed a regression model based on the non-dimensional design procedure described here. In this model the yield force of all shear connectors in one vertical joint is found in a closed form equation followed by the area of post-tensioning steel. The calculated values of the shear force and the area of the post-tensioning steel are based on the PRESSS procedure and yield optimum combination. Moreover, it was shown that the results based on the regression model accurately compare with the iterative PRESSS procedure.

The main objective of this study is to develop an accurate computational model with a wider range of applicability for the optimum design of unbonded post-tensioned coupled precast concrete wall system. An Artificial Neural Network model is proposed to predict the optimum non-dimensional parameters (ρ_1, ρ_2 and ω) related to the optimum required area of the post-tensioning reinforcement (A_p), the total yield force of all shear connectors in one vertical joint (F_{sc}), and the ratio of moment resisted by shear connectors to the design moment (M_{sc}/M_{des}), respectively.

2. Details of unbonded post-tensioned coupled precast concrete wall systems

A typical unbonded post-tensioned coupled precast concrete wall system consists of two or more wall panels with each panel connected to the adjacent panel(s) along a vertical joint with energy dissipating connectors and each wall panel is connected to the foundation with unbonded vertical post-tensioning reinforcement tendons. The connectors which are located along the vertical joint provide additional lateral resistance by shear coupling between the two adjacent panels in addition to energy dissipation. The first wall panel is called the leading wall and the last wall panel is called the trailing wall. The rest of the wall panels, in a three- or more wall panel system, are called intermediate walls. Usually the walls have the same dimensions in order to simply the design. Fig. 1 shows the geometry and the free body diagram of a three-panel wall system. Fig. 1(a) shows the elevation of the wall system and Fig. 1(b) shows the reinforcement details. The wall has a total height of h_w, width l_w and thickness t_w. The total gravity load from all floors including panel weight is W. The post-tensioning reinforcement area is A_p and the total yield force of all shear connectors in a vertical joint is F_{sc}. The interface rotation at design limit state is termed the design angle θ_{des}.

From equilibrium of forces in the horizontal and vertical directions as well as moment equilibrium of each wall panel (Fig. 1(a))

$$V_{des} = \mu \sum P_{des} \tag{1}$$

$$C_{des} = P_{des} + W + F_{scL} - F_{scR} \tag{2}$$

$$M_{capacity,wall} = \sum M_{capacity,panel} \tag{3}$$

where

V_{des} = design base shear
P_{des} = force in the post-tensioning tendon at design drift
μ = coefficient of friction against concrete
C_{des} = compressive reaction on one wall panel at design drift
F_{scL} = total yield force of all shear connectors in joint to left of panel
F_{scR} = total yield force of all shear connectors in joint to right of panel
$M_{capacity,wall}$ = total moment capacity of the wall
$M_{capacity,panel}$ = moment capacity of each panel

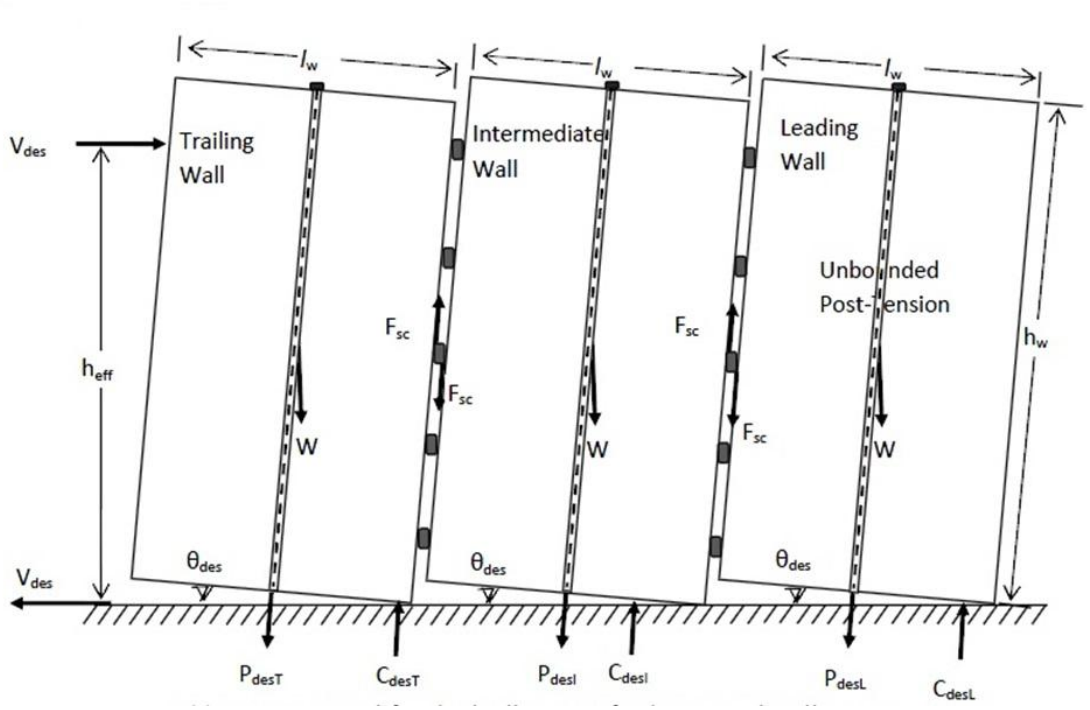

(a) Geometry and free body diagram of a three-panel wall system

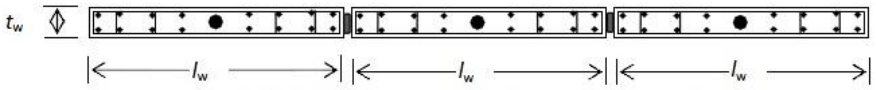

(b) Reinforcement details of a three panels wall

Fig. 1 Elevation and section views of unbonded post-tensioned coupled precast concrete wall system

Given wall geometry, concrete, and post-tensioning reinforcement material properties, the design objectives is to determine the area of the post-tensioning reinforcement (A_p), the total yield force of all shear connectors in one vertical joint (F_{sc}), and the ratio of moment resisted by shear connectors to the design moment (M_{sc}/M_{des}). Several design procedures have been suggested to design the precast post-tensioned concrete wall system and a brief description of each one of these methods is described here.

3. Design procedures for the unbonded post-tensioned coupled precast concrete wall system (PRESSS procedure)

Stanton and Nakaki (2002) developed design guidelines for unbonded post-tensioned (PT) coupled concrete wall systems. The major objective of the PRESSS design guidelines is to minimize the peak drift and to maintain zero residual drift in the wall system after a seismic event. This design objective could be achieved by finding the optimum ratio of the moment

resisted by the shear connectors to the total moment resisted by the wall. The developed design procedure is iterative and lengthy. The iterative nature of the design process is due to the incompatibility of strain in the system as a result of unbonding the post-tensioning tendons from the concrete. The design procedure requires 11 steps to calculate the optimum area of PT reinforcement and shear connectors force. The forces and design moments of the wall panels are calculated based on deformation compatibility and equilibrium. Details of the design procedure and equations along with their derivation for this wall system could be found in the original PRESSS report (Stanton and Nakaki 2002).

3.1 ACI- ITG-5.2-09 simplified procedure

Aaleti and Sritharan (2009) proposed a non-iterative procedure for the design of this wall system. The ACI-ITG-5.2-09 adopted this procedure with some modifications. This procedure, unlike the original PRESSS procedure, does not yield an optimum solution. Also, it always overestimates the area of post-tensioning steel. While any combination of post-tensioning force and shear force in the vertical connectors can be used to resist the required design moment, only one combination yields an optimum solution. A brief summary of this procedure is given below:

Step 1: Define wall dimensions and material properties. The material properties include the modulus of elasticity and the yield strength of the post-tensioning steel as well as the strength of the concrete. Consistent with the PRESSS recommendations all wall segments are assumed to have equal length and equal amounts of post-tensioning steel for the simplicity of the design.

Step 2: Calculate the number of energy dissipating shear connectors in each vertical joint. The ACI-ITG-5.2-09 procedure provides an equation that depends on the nominal capacity of the wall system, the number of wall panels, the shear force of the energy dissipating connector, and the length of each wall panel.

Step 3: Calculate the design moment for the wall panel providing the larger or largest resistance. This is the leading wall in a two-wall system and the intermediate wall for a multi-wall system with three or more panels. The ACI-ITG-5.2-09 procedure provides an equation that depends on the ultimate required moment for the wall system, the number of wall panels, the shear force capacity provided in a vertical joint which is provided by the shear connectors, and the length of each wall panel.

Step 4: Calculate the area of the post-tensioning steel using the moment equilibrium for the forces acting on the base of the wall providing the larger or largest resistance as described in step 3.

Step 5: Estimate the depth of the neutral axis at the base of the trailing wall at the design drift and then assuming that the stress in the post-tensioning steel reaches 95% of the yield stress, the initial stress in the post-tensioning steel is then calculated.

It is important to note that the equations mentioned in steps 2 and 3 above are intended to simplify and get rid of the iterative nature of the PRESSS design procedure. This simplification, however, does not yield an optimum design and requires larger amounts of post-tensioning steel and smaller shear connectors force when compared to the PRESSS procedure.

3.2 Non-dimensional procedure

In a previous study the authors (Saqan and Hawileh 2010) re-investigated the design procedure for such a wall system. They developed a set of non-dimensional charts and parameters for the

design of such walls that require no iterations. Such charts are based on an optimum design of zero residual drift while the moment capacity of the wall is equal to the applied design moment. To generate the design charts, non-dimensional parameters were varied in an extensive parametric study involving an optimization process. The resulting non-dimensional parameters and equations study helped generate user-friendly design charts, applicable to most cases. The three non-dimensional parameters used are the post-tensioning reinforcement ratio (ρ_1), the ratio of the total yield force of all shear connectors in one vertical joint to the force on concrete wall (ρ_2), and the ratio of moment resisted by shear connectors to the design moment (ω). Eq. (4), (5) and (6) define these non-dimensional parameters.

$$\rho_1 = \frac{A_p}{l_w t_w} \tag{4}$$

$$\rho_2 = \frac{F_{sc}}{l_w t_w f_c'} \tag{5}$$

$$\omega = \frac{M_{sc}}{M_{des}} \tag{6}$$

where

A_p = area of post-tensioning tendon reinforcement
l_w = horizontal length of one wall panel
t_w = thickness of the wall
F_{sc} = total yield force of all shear connectors in one vertical joint
f_c' = smaller of the compressive strengths of grout bed and wall concrete
M_{sc} = moment resisted by shear connectors
M_{des} = design moment

Saqan and Hawileh (2010) generated a non-dimensional design equation, besides other equations, that depends on the geometry of the wall; material properties; level of prestress; area of the tendon; capacity of the shear connectors; self-weight of the wall; and any superimposed gravity load, design loads, and drifts. These equations, when properly satisfied, will produce the optimum solution. The equations have been represented in chart formats to easily find the optimum design. However, as always, charts have limitations because they are applicable for certain range of parameters.

The non-dimensional formulation has been used with PRESSS program procedure to generate optimum solutions for a wide range of practical cases. The data generated for the optimum solutions are then used for the Artificial Neural Network model.

3.3 Artificial neural network model

Expert Systems and Artificial Neural Network (ANN) are two of the main branches of artificial intelligence that found many applications in several areas, including civil engineering. ANN consists of massive parallel computational processing elements (neurons) that are connected with weighted connections and have learning capability that simulates the behavior of a brain (Haykin 1999). Several neural network architectures with different learning algorithms, including back-

propagation, were used over the years in different structural engineering applications (Abdalla and Hawileh 2013; Pendharkaeal *et al*. 2011, Zhou *et al*. 2010; Abdalla *et al*. 2007). In this investigation a Multi-Layer Perceptron, Feed-Forward ANN with one hidden layer and back-propagation learning algorithm is employed. The network weights and the network threshold values were initially set to random values and new values of the network weights and bias values are computed during the network training phase. The neurons output are calculated using Eq. (7) as follows

$$y_i = F\left(\sum (x_j \times w_{ij}) + b_j\right) \tag{7}$$

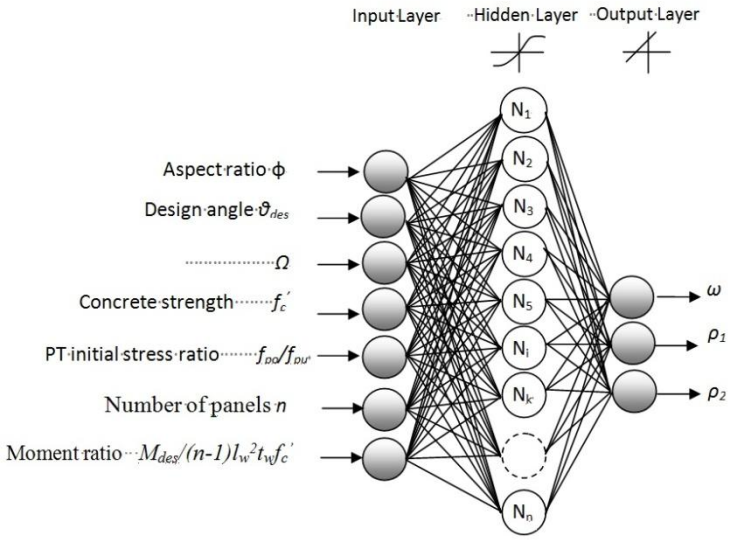

Fig. 2 ANN Architecture

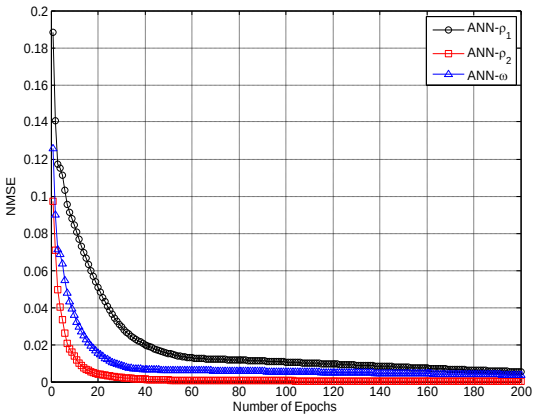

Fig. 3 Learning rate of ANN-ρ_1, ANN- ρ_2 and ANN-ω for training set

where y_i is the output of the neuron i, x_j are the input of j neurons of the previous layer; value w_{ij} is the neuron weights, b_j is the bias for modeling the threshold; and F is the transfer function (Haykin 1999, Abdalla *et al*. 2007, Abdalla and Hawileh 2013). Fig. 2 shows the ANN architecture used in this study with eight input parameters and three output parameters, where:

ϕ = ratio of h_w to l_w

θ_{des}= drift design angle

Ω = ratio of $h_w(\gamma_c + \gamma_L)$ to f_c' = $\dfrac{h_w(\gamma_c + \gamma_L)}{f_c'}$

γ_L = ratio of w_{floor} to $t_w h_w$ and w_{floor} = distributed vertical load on the wall, at base, from all floors

γ_c = density of concrete

f_{po}/f_{pu}= ratio of initial stress after all losses to ultimate stress of post-tensioning steel

n = number of wall panels

The data set used to train the ANN is 345 and to test ANN is 61. The testing data is randomly selected from the total data set. The range of values of the input and output parameters of the training and testing data are listed in Table 1. Three ANN models, mainly ANN - ρ_1, ANN - ρ_2 and ANN-ω were trained using 10 runs with 5000 epoch for each run (Neurosolutions 2010).

Table 1 Range of training and testing data for the ANN model

Parameter	Training data		Testing data	
	Max.	Min.	Max.	Min.
Aspect ratio ϕ $(h_w/l_w))$	10	3.2	10	3.5
Design angle θ_{des}	3	0.5	3	0.5
Load ratio Ω	0.1	0.01	0.1	0.01
Concrete strength f_c'(ksi)	8	4	8	5
PT initial stress ratio f_{po}/f_{pu}	0.65	0.5	0.65	0.5
Number of panels n	5	2	5	2
$\rho_2/\omega = (M_{des}/(n\text{-}1)l_w^2 t_w f_c')$	0.237	0.040	0.258	0.083
ρ_1	0.004	0.00058	0.004	0.001
ρ_2	0.113	0.022	0.124	0.039
ω	0.494	0.450	0.491	0.453

Table 2 Training details and resulted NMSE for training of ANN models

ANN type	Training minimum		Training best network		
	Average NSME	Standard deviation	Run #	Epoch #	Final NMSE
ANN - ρ_1	0.0003311	0.0000995	1	5000	0.0001952
ANN - ρ_2	0.0000255	0.0000032	2	5000	0.0000198
ANN - ω	0.0009907	0.0001860	2	5000	0.0008053

The learning rate coefficient (step size) used for the input and hidden layers was 1.0 and that for output layers was 0.1 for all ANN models. The momentum factor for ANN models was 0.7 and the number of processing elements for the input layer for each ANN was eight while it was 4 for the hidden layers and one for the output layer. The trained ANN models were tested using the randomly test data. The results of ANN prediction are presented in the following section.
Table 2 shows the average and the standard deviation of the minimum Normalized Mean Square Error (NMSE) of the training data and the corresponding final NMSE for the best run among the 10 different runs of each ANN model. It is observed that ANN- ρ_2 has the smallest value of average of minimum NMSE and similarly its best performing run showed the smallest minimum NMSE among other best runs of the three ANN models.

Fig. 3 shows the three best runs learning rate of the training data for the three ANN models. There is sharp decrease in NMSE for all ANN models during the first 20 epochs. As observed from Fig. 3 ANN-ρ_2 showed the fastest learning rate (less NMSE) in the first 200 epochs followed by ANN-ω while ANN-ρ_1 showed the slowest learning rate in the first 200 epochs, however, it did better than ANN-ω afterward. As the number of epochs increases, NMSE for all ANN models decreased at very slow rate and almost remained constant towards the end of the epochs.

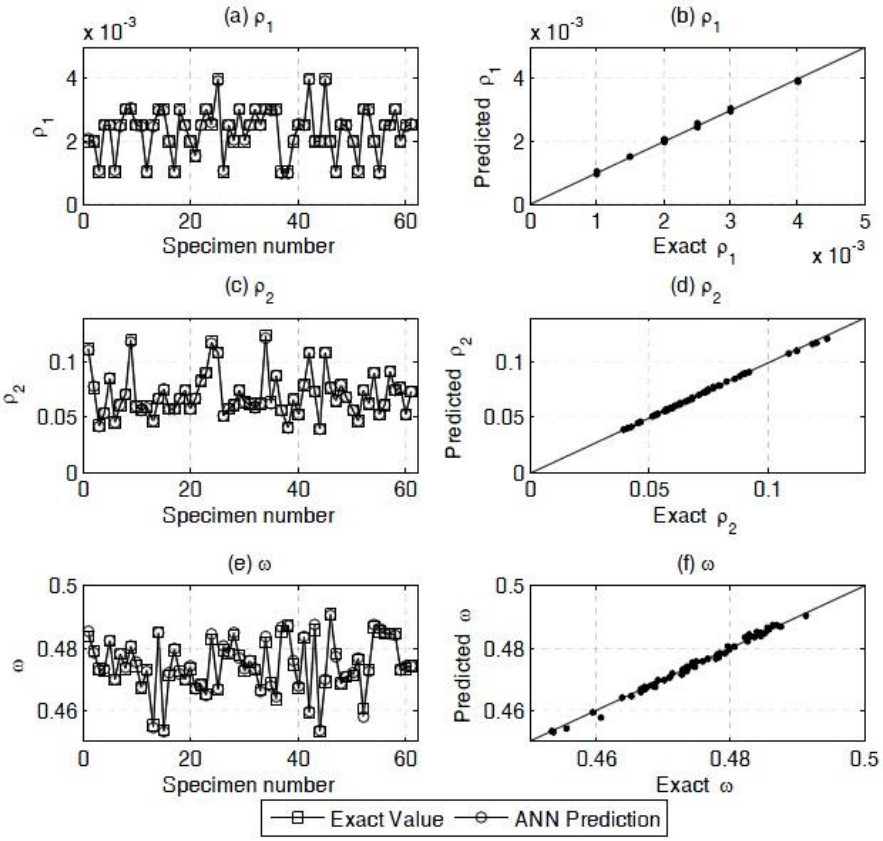

Fig. 4 Accuracy and prediction of ρ_1, ρ_2 and ω using ANN Models

4. ANN model testing, results and discussion

Sixty two data sets were randomly selected for testing the trained ANN models. Several statistical measures have been used to measure the performance of the ANN models as compared to the exact values of the PRESSS procedure. Table 3 shows the performance of the three ANN models on the testing data set. The statistical measures used to compare the performance of the models are given in Eqs. (8) through (12).

Root Mean Square Error (RMSE) is given by

$$\mathrm{RMSE} = \sqrt{\frac{1}{\mathrm{N}}\sum_{\mathrm{i=1}}^{\mathrm{N}}(\mathrm{y_{p,i}} - \mathrm{y_{m,i}})^2} \tag{8}$$

Mean absolute percentage error (MAPE) is given by

$$\mathrm{MAPE} = \frac{1}{\mathrm{N}}\sum_{\mathrm{i=1}}^{\mathrm{N}}\left|((\mathrm{y_{p,i}} - \mathrm{y_{m,i}})/\mathrm{y_{m,i}})\times 100\%\right| \tag{9}$$

Absolute error (MAE) is given by

$$\mathrm{MAE} = \frac{1}{\mathrm{N}}\sum_{\mathrm{i=1}}^{\mathrm{N}}\left|(\mathrm{y_{p,i}} - \mathrm{y_{m,i}})\right| \tag{10}$$

Normalized mean square error (NMSE) is given by

$$\mathrm{NMSE} = \frac{\sum_{\mathrm{i=1}}^{\mathrm{N}}(\mathrm{y_{p,i}} - \mathrm{y_{m,i}})^2}{\sum_{\mathrm{i=1}}^{\mathrm{N}}(\overline{\mathrm{y}}_{\mathrm{m,i}} - \mathrm{y_{m,i}})^2} \tag{11}$$

Correlation coefficient (r) is given by

$$\mathrm{r} = \frac{\frac{1}{\mathrm{N}}\sum_{\mathrm{i=1}}^{\mathrm{N}}(\overline{\mathrm{y}}_{\mathrm{m,i}} - \mathrm{y_{m,i}})(\overline{\mathrm{y}}_{\mathrm{p,i}} - \mathrm{y_{p,i}})}{\sqrt{\frac{1}{\mathrm{N}}\sum_{\mathrm{i=1}}^{\mathrm{N}}(\overline{\mathrm{y}}_{\mathrm{m,i}} - \mathrm{y_{m,i}})^2}\times\sqrt{\frac{1}{\mathrm{N}}\sum_{\mathrm{i=1}}^{\mathrm{N}}(\overline{\mathrm{y}}_{\mathrm{p,i}} - \mathrm{y_{p,i}})^2}} \tag{12}$$

where N is the number of data items, y_m are the exact values of ρ_1, ρ_2 and ω from PRESSS procedure and y_p are the ANN predicted values of ρ_1, ρ_2 and ω and $\bar{y}_m$, $\bar{y}_p$ are their averages, respectively.

It is observed from Table 3 that ANN predictions of ρ_1, ρ_2 and ω are very accurate with the MAPE range between 0.13% and 1.22% and correlation coefficients of more than r = 0.99.

Table 3 Summary of performance of the ANN model on testing data

Performance criterion	Testing data		
	ρ_1	ρ_2	ω
Root mean square error (RMSE)	0.000034	0.000556	0.000815
Mean absolute error (MAE)	0.000025	0.000315	0.000623
Mean absolute percent error (MAPE) (%)	1.216402	0.384974	0.131189
Minimum absolute percent error (%)	0.028951	0.002018	0.002663
Maximum absolute percent error (%)	2.716151	2.142832	0.546785
Normalized mean square error (NMSE)	0.002020	0.000779	0.009139
Correlation coefficient (r)	0.999112	0.999749	0.996557

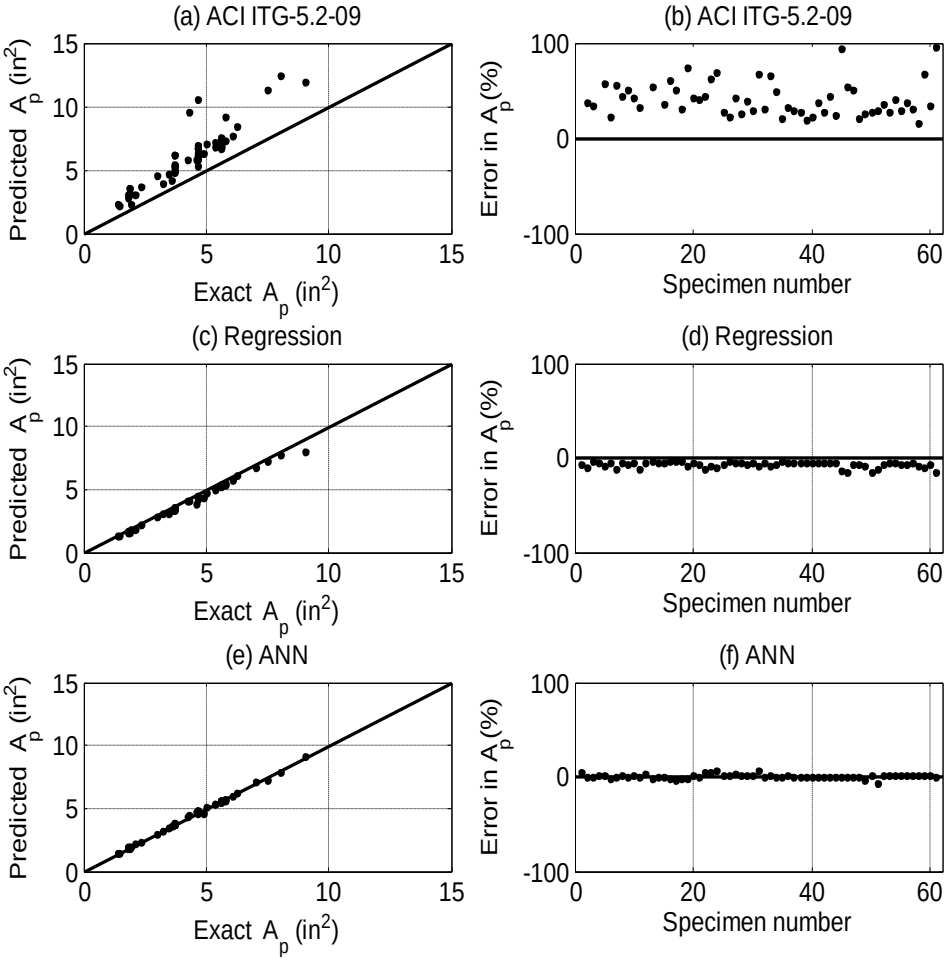

Fig. 5 Accuracy and error in prediction of area of post-tensioning reinforcement (A_p)

Table 4 Summary of performance of all procedures on prediction of A_p

Performance criterion	ACI ITG-5.2-09 Procedure	Regression model	ANN model
Root mean square error (RMSE) (in^2)	2.609554	0.307137	0.086433
Mean absolute error (MAE) (in^2)	2.008832	0.274707	0.062886
Mean absolute percent error (MAPE) (%)	47.35974	6.805871	1.557159
Minimum absolute error (in^2)	0.386142	0.109494	0.000342
Maximum absolute error (in^2)	10.36757	1.056679	0.320003
Normalized mean square error (NMSE)	2.610513	0.036162	0.002864
Correlation coefficient (r)	0.681198	0.979852	0.998689

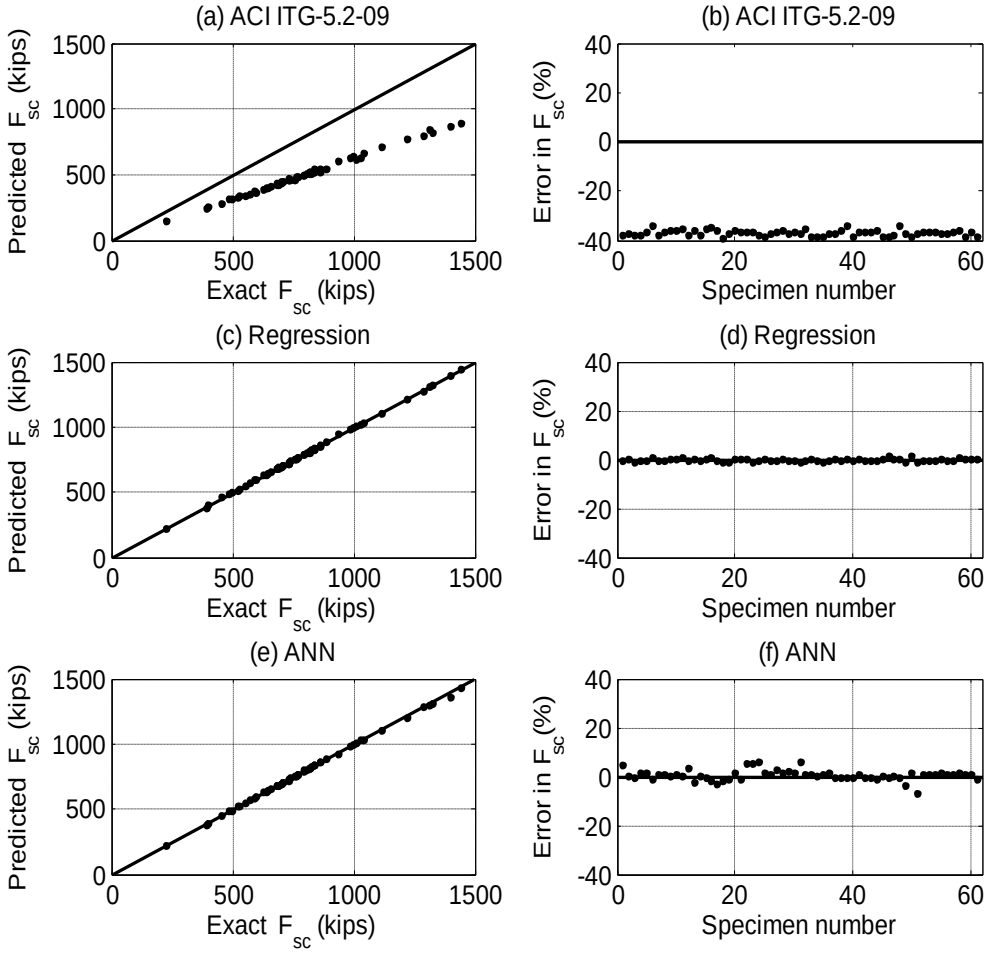

Fig. 6 Accuracy and error in prediction of shear connectors force (F_{sc})

Table 5 Summary of performance of all procedures on prediction of F_{sc}

Performance criterion	ACI ITG-5.2-09 Procedure	Regression Model	ANN Model
Root mean square error (RMSE) (kips)	320.1336	4.431357	6.429312
Mean absolute error (MAE) (kips)	301.5992	3.360171	3.712003
Mean absolute percent error (MAPE) (%)	36.79152	0.438112	0.396110
Minimum relative error (kips)	75.77773	0.011863	0.000071
Maximum relative error (kips)	631.2267	12.9505	29.23712
Normalized mean square error (NMSE)	1.238078	0.000237	0.000499
Correlation coefficient (r)	0.516142	0.999874	0.999815

The most accurate prediction, however, is that of ANN-ρ_2 with r = 0.9997, NMSE = 0.00078 and MAPE = 0.385%, as shown in Table 3.

Fig. 4 shows a comparison of prediction between the exactly calculated values of the non-dimensional parameters ρ_1, ρ_2 and ω and the ANN predicted ones. It also shows the accuracy of the ANN models in predicting these test data sets. Fig. 4(a) shows the ANN-ρ_1 model predictions of ρ_1 while Fig. 4(b) shows the accuracy of ANN-ρ_1 in predicting the test data as compared to the PRESSS exact values of ρ_1. Fig. 4(c) shows the ANN-ρ_2 predictions of ρ_2 while Fig. 4(d) shows the accuracy of ANN-ρ_2 in predicting the test data as compared to the PRESSS exact values of ρ_2. Fig. 4(e) shows the ANN- ω predictions of ω while Fig. 4(f) shows the accuracy of ANN- ω in predicting the test data as compared to the PRESSS exact values of ω. It is clear from Fig. 4(c) and Fig. 4(d) that ANN-ρ_2 model shows the best fit among all ANN models.

Sixty two testing data sets were used to predict ρ_1 and ρ_2 values using the trained ANN Model. The Regression Model was also used to predict the non-dimensional parameters ρ_1 and ρ_2 based on the 62 testing data sets. The predicted non-dimensional parameters, ρ_1 and ρ_2, were then used to calculate the post-tensioning reinforcement area (A_p) and the shear connectors force (F_{sc}) using specified material properties and design parameters, given in Table 6, for the jointed precast wall systems. The exact PRESSS Procedure and the ACI ITG-5.2-09 Procedure were also used to calculate the post-tensioning reinforcement area (A_p) and the shear connectors force (F_{sc}) using the same specified material properties and design parameters for the jointed precast wall systems. The ACI ITG-5.2-09 Procedure, Regression Model and ANN Model results were compared with the exact PRESSS Procedure results and their performances were measured.

Table 4 shows the performance of the three methods in predicting the post-tensioning reinforcement area (A_p) based on the given statistical performance. It is observed from Table 4 that ANN predictions of A_p are very accurate compared to the two other methods with MAPE = 1.56%, NMSE = 0.00286 and r = 0.9987. The ACI ITG-5.2-09 procedure has the poorest performance with MAPE = 47.36%, NMSE = 2.61 and r = 0.6812, as shown in Table 4.

Fig. 5 shows a comparison of prediction between the exact values of A_p using PRESSS procedure, ACI ITG-5.2-09 procedure, Regression Model and ANN Model. It also shows the relative percent error of the three methods in predicting these test data sets. It is clear from Fig. 5(e) and Fig. 5(f) that ANN model predictions are the most accurate while ACI ITG-5.2-09 procedure results are the least accurate as shown in Fig. 5(a) and Fig. 5(b).

Table 5 shows the performance of the three methods in predicting the shear connectors force (F_{sc}) based on the given statistical performance. It is observed from Table 5 that the ANN Model

and the Regression Model predictions of F_{sc} are very accurate compared to the ACI ITG-5.2-09 Procedure with MAPE equal to 0.396% and 0.438%, respectively, NMSE equal to 0.000499 and 0.000237, respectively and correlation coefficient equal to 0.99982 and 0.9999, respectively. The ACI ITG-5.2-09 procedure has the poorest performance with MAPE = 36.79%, NMSE = 1.24 and r = 0.516, as shown in Table 5.

Fig. 6 shows a comparison of prediction between the exact values of F_{sc} using PRESSS Procedure, ACI ITG-5.2-09 procedure, Regression Model and ANN Model. It also shows the relative percent error of the three methods in predicting these test data sets. It is clear from Fig. 6(c) and Fig. 6(d) that Regression Model predictions are the most accurate, followed by the ANN Model (Fig. 6(e) and Fig. 6(f)) while ACI ITG-5.2-09 Procedure results are the least accurate as shown in Fig. 6(a) and Fig. 6(b).

5. Parametric study

Using the developed ANN model a parametric study was conducted to study the effect of the various design parameters on the coupled wall system design.

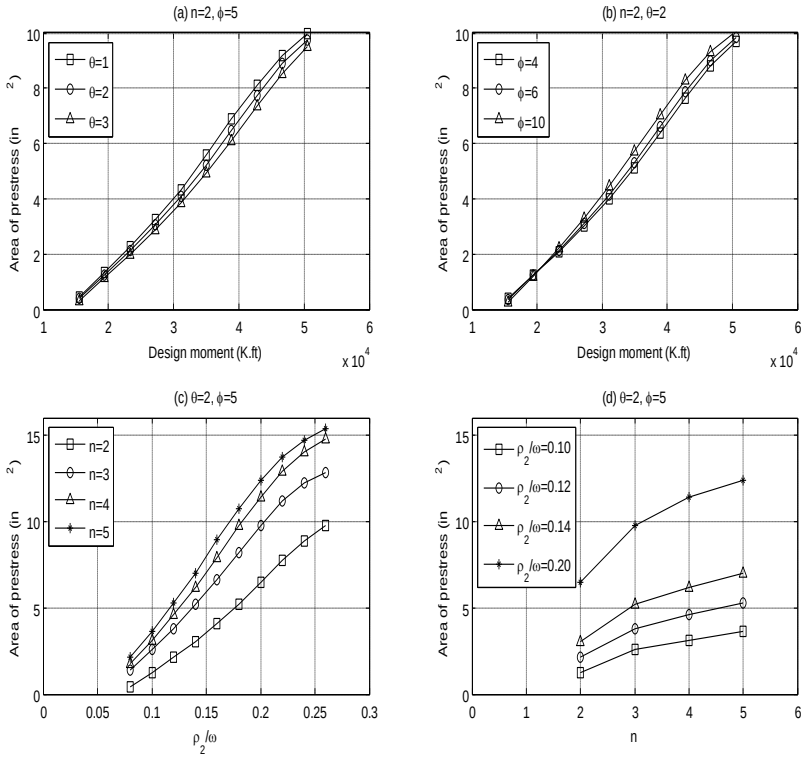

Fig. 7 Area of post-tensioning reinforcement (Ω = 0.04, f'_c = 6, f_{po}/f_{pu}= 0.6)

5.1 Effect of design angle (θ), aspect ratio ($\phi = h_w/l_w$), number of panels (n) and design moment on post-tensioning reinforcement area

Fig. 7(a) shows the effect of design angle (θ) on post-tensioning reinforcement area (A_p) for two panels n = 2 and aspect ratio $\phi = h_w/l_w = 5$. As expected, as the design moment increases, the post-tensioning reinforcement increases. The variation on design angle (θ) has little effect on post-tensioning reinforcement (A_p), especially for a small design moment. The influence of the design angle on the post-tensioning reinforcement area is more apparent for larger design moments,however, it is still small. Similar observation can be made about the post-tensioning reinforcement (A_p) when the aspect ratio (ϕ) is varied as can be deduced from Fig. 7(b).

Fig. 7(c) shows the effect of the number of panels (n) on post-tensioning reinforcement area (A_p) for design angle θ = 2% and aspect ratio $\phi = h_w/l_w = 5$. It is observed from Fig. 7(c) that, as the number of panels increases, the post-tensioning reinforcement area (A_p) increases, however, the effect of the number of panels becomes smaller when n = 4 or higher. It must be noted that the total area of post-tensioning steel for the entire wall will substantially increase as n increases. For example, in a three- versus two-panel walls it is not only that (A_p) in each panel increases as shown in Fig. 7(c) but also it will be provided in three panels rather than only two. Fig. 7(d) shows the effect of moment factor (ρ_2/ω) on post-tensioning reinforcement area (A_p) also for design angle θ = 2% and aspect ratio $\phi = h_w/l_w = 5$. As the moment factor (ρ_2/ω) increases the post-tensioning reinforcement area increases.

5.2 Effect of design angle (θ), aspect ratio ($\phi = h_w/l_w$), number of panels (n) and design moment on shear connectors' force

Fig. 8(a) shows the effect of design angle (θ) on shear connectors force (F_{sc}) for two panels n = 2 and aspect ratio $\phi = h_w/l_w = 5$. As expected, as the design moment increases, the shear connectors force increases. The variation on design angle (θ) has little effect on shear connectors force (F_{sc}), especially for a small design moment. The influence of the design angle on the magnitude of shear connectors force is more apparent for larger design moments, however, it is still small. Similar observation can be made about the shear connectors force (F_{sc}) for the variation of aspect ratio (ϕ) as can be deduced from Fig. 8(b).

Fig. 8(c) shows the effect of the number of panels (n) on shear connectors force (F_{sc}) for design angle θ = 2% and aspect ratio $\phi = h_w/l_w = 5$. It is observed from Fig. 8(c) that, the number of panels has no influence on the shear connectors force in one vertical joint, however, the total shear connectors force will substantially increase since in three-panel wall two vertical joints exist versus only one joint in two-panel wall. Fig. 8(d) shows the effect of moment factor (ρ_2/ω) on shear connectors force (F_{sc}) also for design angle θ = 2% and aspect ratio $\phi = h_w/l_w = 5$. As the moment factor (ρ_2/ω) increases the shear connectors force increases.

Fig. 9(a) shows the effect of design angle (θ) on moment ratio (ω) for two panels n = 2 and aspect ratio $\phi = h_w/l_w = 5$. The moment ratio (ω) varies nonlinearly with the design moment for a given design angle and reaches a minimum at a certain design moment. As the design angle decreases, the moment ratio (ω) increases. Fig. 9(c) shows the effect of aspect ratio (ϕ) on moment ratio (ω) for two panels n = 2 and design angle θ = 2%. Similarly, the moment ratio (ω) varies nonlinearly with the design moment for a given design angle and reaches a minimum at a certain design moment. As the aspect ratio decreases, the moment ratio (ω) decreases. Similar observation can be made about the moment

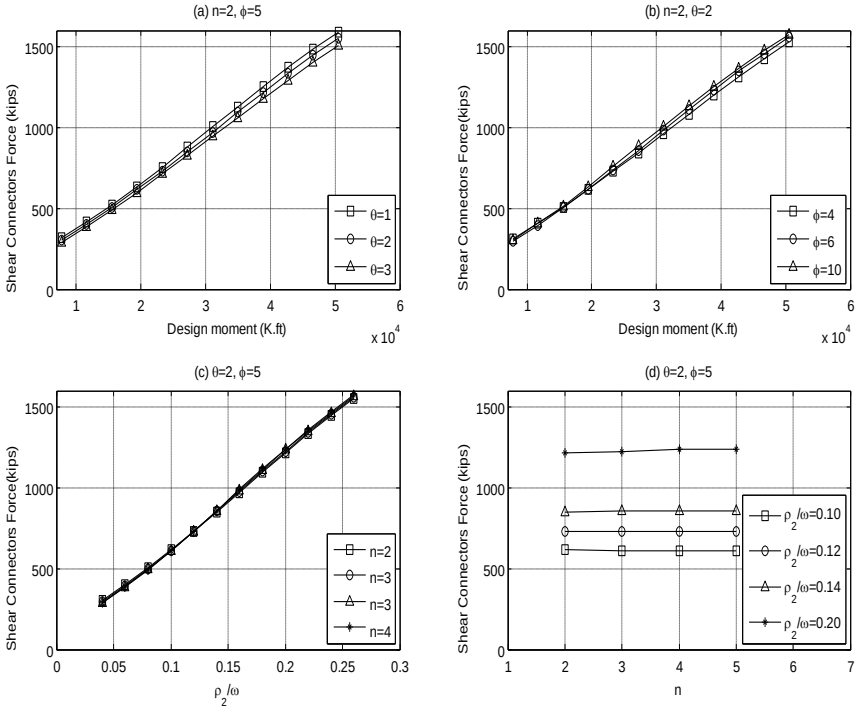

Fig. 8 Shear connectors force ($\Omega = 0.04$, $f'_c = 6$, $f_{po}/f_{pu} = 0.6$)

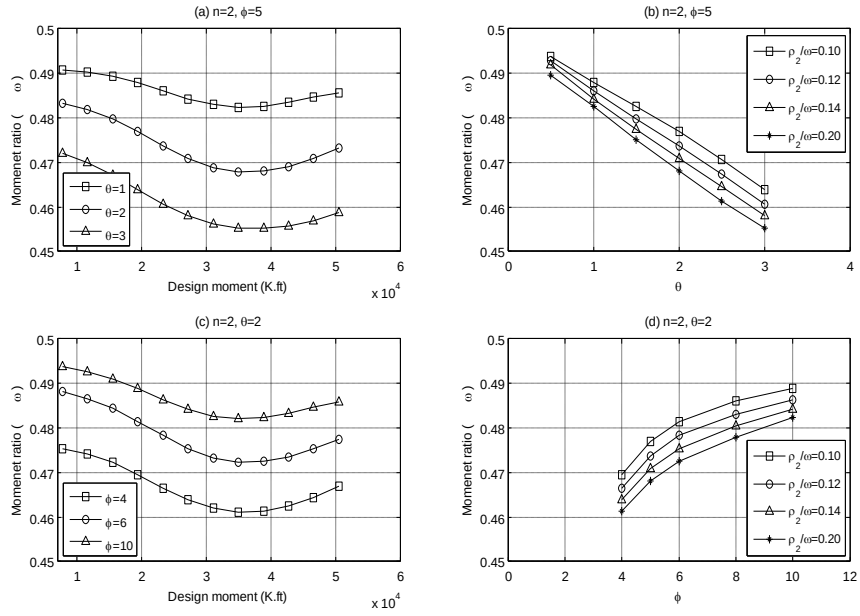

Fig. 9 Moment ratio ($n = 2$, $\phi = 5$, $\theta = 2$, $\Omega = 0.04$, $f'_c = 6$, $f_{po}/f_{pu} = 0.6$)

ratio (ω) for the variation of aspect ratio (ϕ) as can be deduced from Fig. 9(c).

Fig. 9(b) shows the variation of moment ratio (ω) with the design angle for number of panels n = 2 and aspect ratio $\phi = h_w/l_w = 5$. As shown, the moment ratio (ω) varies almost linearly with the design angle for a given moment factor (ρ_2/ω). As the design angle increases the moment ratio decreases. Fig. 9(d) shows the variation of moment ratio (ω) with the aspect ratio (ϕ) for number of panels n = 2 and design angle θ = 2%. As shown, the moment ratio (ω) varies nonlinearly with the aspect ratio and for a given moment factor (ρ_2/ω), as the aspect ratio increases the moment ratio increases.

6. Design examples

This section presents twelve examples with different number of panels (2, 3, 4 and 5) for the design of precast coupled wall system. Table 6 shows the material properties and design parameters for the twelve examples of the coupled precast wall system. The wall height (h_w), wall length (l_w), wall thickness (t_w), concrete properties (f'_c, γ_c), post-tensioning reinforcement properties (f_{py}, f_{pu}, E_p), post-tensioning ratio (f_{po}/f_{pu}) and interface rotation at the design drift (θ) are kept constant as shown in Table 6. The number of walls in each system (n) is varied from two to five wall segments. The floor load (W_{floor}), load ratio (Ω), design moment (M_{des}) and moment factor ($M_{des}/(n\text{-}1)l_w^2 t_w f'_c$) are also varied as shown in Table 7. The twelve wall examples were designed according to the ACI ITG-5.2-09 design procedure to obtain the required post-tensioning reinforcement area (A_p) and shear connectors force (F_{sc}) and a strength reduction factor of 1.0 is used in all calculations. These two design parameters are also calculated from the non-dimensional parameters using the Regression Model (Hawileh *et al*. 2013) and the ANN Model presented in this investigation. The results are compared with the original iterative PRESSS procedure which is the exact procedure. Table 7 provides a summary of the design results parameters, the post-tensioning reinforcement area (A_p) and shear connectors force (F_{sc}) which were obtained using

Table 6 Material properties and design parameters for the design examples of the jointed precast walls system

Parameter	Value	Comments
h_w, in (m)	780 (19.5)	Wall height
l_w, in (m)	156 (3.9)	Length of one wall segment
t_w, in (m)	12 (0.3)	Wall thickness
f'_c, ksi (MPa)	6 (41.4)	Concrete compressive strength
γ_c, pcf (kN/m^3)	145 (22.8)	Unit weight of concrete
f_{py}, ksi (MPa)	240 (1654)	Yield stress of post-tensioning reinforcement
f_{pu}, ksi (MPa)	270 (1860)	Ultimate stress of post-tensioning reinforcement
E_p, ksi (GPa)	28500 (196)	Modulus of elasticity of post-tensioning reinforcement
f_{po}/f_{pu}	0.6	Ratio of initial stress after all losses to ultimate stress of post-tensioning steel
ϕ	5	Wall aspect ratio, i.e., ratio of h_w to l_w
θ_{des}, %	2	Interface rotation at the design drift

Table 7 Summary of the twelve design examples of the jointed precast wall system showing relative percent error

		n = 2			***n = 3***			***n = 4***			***n = 5***		
		Case 1	Case 2	Case 3	Case 1	Case 2	Case 3	Case 1	Case 2	Case 3	Case 1	Case 2	Case 3
Load Ratio, Ω		0.03	0.04	0.05	0.03	0.04	0.05	0.03	0.07	0.08	0.05	0.07	0.09
$M_{des}/(n\text{-}1)l_w^2 t_w f'_c$		0.18867	0.23106	0.13605	0.13385	0.14384	0.10632	0.13340	0.11545	0.16305	0.13062	0.10888	0.15052
M_{des}, k.in (kN.m)		330584 (37349)	404868 (45742)	238384 (26932)	469073 (53009)	504068 (56964)	372583 (421005)	704352 (79598)	606870 (68581)	857084 (96857)	915479 (103457)	763117 (86238)	1054955 (119219)
W_{floor}, k/in (kN/m)		1.39 (243.5)	2.11 (369.5)	2.83 (495.6)	1.39 (243.5)	2.11 (369.5)	2.83 (495.6)	1.39 (243.5)	4.27 (747.7)	4.99 (873.8)	2.83 (495.6)	4.27 (747.7)	5.71 (999.8)
PRESSS procedure	A_p, in.^{2} (cm^2) (%error)	5.61 (36.2)	7.48 (48.3)	1.86 (12.0)	4.65 (30.0)	4.65 (30.0)	1.84 (11.9)	5.58 (36.0)	1.84 (11.9)	4.65 (30.0)	4.65 (30.0)	1.84 (11.9)	3.71 (23.9)
	F_{sc}, kip (kN) (%error)	982.4 (4369.7)	1217.1 (5413.7)	730.4 (3248.8)	701.4 (3120.0)	760.7 (3383.6)	572.9 (2548.3)	705.2 (3136.7)	629.6 (2800.5)	885.2 (3937.4)	698.0 (3104.7)	594.0 (2642.1)	821.7 (3655.0)
ACI ITG-5.2-09 procedure	A_p, in.^{2} (cm^2) (%error)	7.62 (49.2) (35.8%)	11.33 (73.1) (51.5%)	3.23 (20.8) (73.7%)	5.83 (37.6) (25.4%)	6.01 (38.8) (28.2%)	3.11 (20.1) (69.0%)	6.94 (44.8) (24.2%)	3.57 (23.0) (94.0%)	6.97 (45.0) (49.9%)	6.37 (41.1) (37.0%)	3.60 (23.2) (95.7%)	6.22 (40.1) (67.7%)
	F_{sc}, kip (kN) (%error)	635.4 (2826.3) (35.3%)	778.2 (3461.4) (36.1%)	458.2 (2038.1) (37.3%)	450.8 (2005.2) (36.3%)	484.4 (2154.6) (36.3%)	358.1 (1592.8) (37.5%)	451.3 2007.4) (36.0%)	388.8 (1729.4) (38.2%)	549.1 (2442.4) (38.9%)	439.9 (1956.7) (37.0%)	366.7 (1631.1) (38.3%)	506.9 (2254.7) (38.3)
Regression model	A_p, in.^{2} (cm^2) (%error)	5.35 (34.5) (4.6%)	7.22 (46.6) (3.5%)	1.72 (8.2) (7.5%)	4.41 (28.5) (5.2%)	4.41 (28.5) (5.2%)	1.66 (10.7) (9.6%)	5.32 (34.3) (4.7%)	1.60 (10.3) (13.0%)	4.33 (27.9) (6.9%)	4.35 (28.1) (6.5%)	1.57 (10.1) (14.7%)	3.33 (21.5) (10.2%)
	F_{sc}, kip (kN) (%error)	987.0 (4390.2) (0.5%)	1214.3 (5401.2) (0.2%)	725.4 (3226.6) (0.7%)	701.5 (3120.3) (0.0%)	759.9 (3380.0) (0.1%)	570.7 (2538.5) (0.4%)	702.4 (3124.3) (0.4%)	631.1 (2807.1) (0.2%)	885.5 (3938.7) (0.0%)	697.6 (3102.9) (0.1%)	597.0 (2655.5) (0.5%)	826.7 (3677.2) (0.6%)
ANN model	A_p, in.^{2} (cm^2) (%error)	5.58 (36.0) (0.5%)	7.29 (47.0) (2.5%)	1.84 (11.9) (1.1%)	4.71 (30.4) (1.3%)	4.72 (30.5) (1.5%)	1.95 (12.6) (6.0%)	5.54 (35.7) (0.7%)	1.84 (11.9) (0.0%)	4.67 (30.1) (0.4%)	4.70 (30.3) (1.1%)	1.83 (11.8) (0.5%)	3.76 (24.3) (1.3%)
	F_{sc}, kip (kN) (%error)	984.8 (4380.4) (0.2%)	1209.2 (5378.5) (0.6%)	724.2 (3221.2) (0.8%)	700.2 (3114.5) (0.2%)	761.3 (3386.3) (0.1%)	570.4 (2537.1) (0.4%)	703.3 (3128.3) (0.3%)	630.9 (2806.2) (0.2%)	891.5 (3965.4) (0.7%)	699.0 (3109.2) (0.1%)	594.6 (2644.8) (0.1%)	823.5 (3662.9) (0.2%)

PRESSS procedure, ACI ITG-5.2-09 procedure, Regression Model and ANN Model together with the percent relative error as compared to the exact PRESSS procedure.

It is observed from Table 7 that for the twelve design examples shown the Regression Model and the ANN Model are much more accurate than the ACI ITG-5.2-09 Procedure in predicting the post-tensioning reinforcement area and the shear connectors force when compared to the exact PRESSS procedure. While the relative percent error of the Regression Model and the ANN Model are less than 1% for predicting the shear connectors force in each vertical joint between the precast walls (F_{sc}) as compared to the exact PRESSS procedure results, the relative percent error of the ACI ITG-5.2-09 vary between 35.3% and 38.9%. The ACI ITG-5.2-09 procedure always underestimates the shear connectors force. The ANN Model has best performance in predicting the post-tensioning reinforcement area (A_p) with the relative percent error range between 0%-6% while the Regression Model has relative percent error range between 3.5%-14.7% and the ACI ITG-5.2-09 procedure has relative percent error range between 24.2%-95.7%. The ACI ITG-5.2-09 procedure always overestimates the post-tensioning reinforcement area.

Although any combination of the PT steel and the shear connectors force can be chosen by the designer to achieve a certain moment strength, in general, the optimum design will be achieved by making the connectors force as large as possible. Also, maximizing the connectors force will maximize the damping. However, the largest value of the connectors force must be constrained by the zero residual drift criterion (Stanton and Nakaki 2002) of the wall system after an earthquake.

The ANN Model is trained and tested on results of optimum solution and therefore it provides an optimum solution that minimizes the overall drift in the wall system by maximizing the connectors force while maintaining zero residual drift after a seismic event. The ANN model is simple, non-iterative and easy to use and its design values are accurate and in close agreement with the exact optimum values produced by the lengthy and iterative PRESSS procedure.

7. Conclusions

This paper presented the development of an ANN model that can accurately predict the optimum design parameters for unbonded post-tensioned coupled precast concrete wall system. PRESSS provided an iterative procedure that requires lengthy calculations to achieve an optimum design. ACI ITG-5.2-09 adopted a simplified non-iterative procedure for the design of such wall systems. A non-dimensional procedure and a simplified procedure based on regression analysis were proposed by the authors in a previous research to achieve optimum design with reasonable design steps. For the ANN model the training and testing data were generated based on the PRESSS procedure. A parametric study was then performed using the developed ANN model to investigate the influence of the aspect ratio of wall panels (h_w/l_w), design drift angle (θ_{des}), number of wall panels (n), design moment, and design moment factor (ρ_2/ω) on the area of the post-tensioning reinforcement (A_p) and the shear force of the energy dissipating devices (F_{sc}). Twelve design examples were also presented with different number of panels and the results were in close agreement with the PRESSS procedure. The following conclusions can be drawn from the results of this investigation:

1. ANN predictions of ρ_1, ρ_2 and ω are very accurate with the MAPE range between 0.13% and 1.22% and correlation coefficients almost equal to 1.0. The most accurate prediction, however, is that of ANN-ρ_2 with r = 0.9997, NMSE = 0.00078 and MAPE = 0.385%.

2. The ACI ITG-5.2-09 procedure does not yield optimum values for A_p and F_{sc} with MAPE = 47.36% and 36.79%, respectively, NMSE = 2.61 and 1.24, respectively, and r = 0.6812 and 0.516, respectively.

3. The ANN and Regression Models predictions of F_{sc} are very accurate compared to the exact PRESSS procedure results with MAPE equal to 0.396% and 0.438%, respectively, NMSE equal to 0.000499 and 0.000237, respectively and correlation coefficient almost equal to 1.0 for both procedures.

4. For a given design angle and wall aspect ratio, the number of panels, design moment and moment ratio has noticeable effect on the magnitude of the post-tensioning reinforcement area.

5. For a given number of panels, the design angle and the aspect ratio has very little influence on the post-tensioning reinforcement area.

6. For a given design angle and wall aspect ratio, the design moment and moment ratio has noticeable effect on the magnitude of the shear connectors force.

7. For a given design angle and aspect ratio, the number of panels has no influence on the magnitude of the shear connectors force.

8. While the relative percent error of the ANN Models are less than 1% for predicting Fsc in each vertical joint between the precast walls as compared to the exact PRESSS procedure results, the ACI ITG-5.2-09 procedure underestimates the shear connectors force with relative percent error ranges between 35.3% and 38.9%.

9. Also, while the relative percent error of the ANN Models are between 0%-6% for predicting the post-tensioning reinforcement area, the ACI ITG-5.2-09 procedure overestimates the post-tensioning reinforcement area with relative percent error ranges between 24.2%-95.7%.

References

Abdalla, J.A. and Hawileh, R.A. (2013), Artificial neural network predictions of fatigue life of steel bars based on hysteretic energy, In press, Journal of Computing in Civil Engineering.

Abdalla, J.A., Elsanosi, A. and Abdelwahab, A. (2007), Modeling and simulation of shear resistance of R/C beams using artificial neural network, *J. Franklin Inst.*, **344**(5), 741-756.

Aaleti, S. and Sritharan, S. (2009), A simplified analysis method for characterizing unbonded post-tensioned precast wall systems, *Eng. Struct.*, **31**, 2966-2975.

American Concrete Institute (ACI) Innovation Task Group 5. (2009), Requirements for design of a special unbonded post-tensioned precast shear wall satisfying ACI ITG-5.1 (ACI ITG-5.2-09) and Commentary. ACI ITG-5.2-09, Farmington Hills (MI).

Bhunia, D., Prakash, V. and Pandey, A.D. (2012), "A study on the behaviour of coupled shear walls", *Struct. Eng. Mech.*, **42**(5).

Ghosh, S.K. and Hawkins, N.M. (2003), "Codification of PRESSS structural systems", *PCI J.*, **48**(4), 140-143.

Hawkins, N.M. and Ghosh, S.K. (2004), "Acceptance criteria for special precast concrete structural walls based on validation testing", *PCI J.*, **49**(5), 78-92.

Hawileh, R.A., Saqan, E.I. and Abdalla, J.A. (2013), **"**Simplified optimum design procedure for special unbonded post-tensioned split precast shear walls. Technical Note", *ASCE J. Struct. Eng.*, **139**(2), 294-299.

Hawileh, R.A., Tabatabai, H., Rahman, A. and Amro, A. (2006), "Non-dimensional design procedures for precast, prestressed concrete hybrid frames", *PCI J.*, **51**(5), 110-130.

Nakaki, S.D., Stanton, J.F. and Sritharan, S. (1999), "An overview of the PRESSS five-story precast test building", *PCI J.*, **44**(2), 26-39.

Pendharkar, U., Chaudhary, S. and Nagpal, A.K. (2011), "Prediction of moments in composite frames considering cracking and time effects using Neural Network models", *Struct. Eng. Mech.*, **39**(2), 267-285.
Priestley, M.J.N. (2002), "Direct displacement based design of precast prestressed concrete buildings", *PCI J.*, **47**(6), 66-79.
Priestley, M.J.N. (1996), "The PRESSS program — Current status and proposed plans for phase III", *PCI J.*, **41**(2), 22-40.
Priestley, M.J.N. (1991), "Overview of the PRESSS research program", *PCI J.*, **36**(4), 50-57.
Priestley, M.J.N., Sritharan, S., Conley J.R. and Pampanin, S. (1999), "Preliminary Results and Conclusions from the PRESSS Five-Story Precast Concrete Test Building", *PCI J.*, **44**(6), 42-67.
Saqan, E.I. and Hawileh, R.A. (2010), Non-dimensional design charts for unbonded post-tensioned split precast concrete walls, *PCI J.*, **55**(4), 78-99.
Sritharan, S. and Aaleti, S. (2006), Seismic Design of Jointed Precast Concrete Wall Systems. The 4th International Conference on Earthquake Engineering, Paper No. 268, Taipei, Taiwan.
Stanton, J.F. and Nakaki, S.D. (2002), *Design Guidelines for Precast Concrete Seismic Structural Systems*, PRESSS report No. 01/03-09, PCI, Chicago, IL, and University of Washington report Number SM 02-02, Seattle, WA.
Zhou, G., Pan, D., Xu, X. and Rafiq, Y.M. (2010), "Innovative ANN technique for predicting failure/cracking load of masonry wall panel under lateral load", *J. Comput. Civil Eng.*, **24**(4), 377-387.

CC